Cross-correlation-based Complex-valued Sparse Deconvolution Beamforming for Active Sonar System in Multipath Environment

Quan Tao
School of Marine Science and Technology
Tianjin University
Tianjin, China
TQdidi@tju.edu.cn

Zhiwen Qian
School of Marine Science and Technology
Tianjin University
Tianjin, China
zhiwenqian@tju.edu.cn

Xiaomei Fu *
School of Marine Science and Technology
Tianjin University,
Tianjin, China
fuxiaomei@tju.edu.cn
*Corresponding author

2025 IEEE 14th International Conference on Communications, Circuits and Systems (ICCCAS) | 979-8-3315-4477-5/25/$31.00 ©2025 IEEE | DOI: 10.1109/ICCCAS65806.2025.11102609

***Abstract*—Direction-of-arrival (DOA) estimation is fundamental for marine applications, but it faces significant challenges in multipath environments where the received signals are often coherent. While several algorithms exist for narrowband signals, they struggle with wideband signals widely used in the active sonar system. To address these issues, a cross-correlation-based complex-valued sparse deconvolution beamforming (CC-SDB) is proposed in this paper. To fully utilize the known information of source signal, conventional DOA estimation model is developed with cross-correlation function, thus the output SNR is maximized, and the robustness of wideband beamforming is enhanced. To obtain high-resolution DOA estimation at coherent case, a complex-valued deconvolution algorithm with sparseness and continuity constraints is applied as a post processor in the developed model, thereby suppressing the main-lobe width and sidelobe level. Numerical simulations and underwater experiments validate the algorithm's effectiveness.**

Keywords—Array signal processing, multipath effect, sparse deconvolution.

I. INTRODUCTION

Array signal processing is a key technology in radar and terrestrial communication systems [1, 2]. In the terrestrial application, millimeter wave radar sensors have been used for non-contact heart rate and respiratory rate measurement through clothing with microwave Doppler sensors recently [3]. With the development of marine applications, such as sunken ship localization, offshore activities and underwater target identification, underwater direction-of-arrival (DOA) estimation has become increasingly attractive during the last decade [4, 5]. However, the complex underwater channel environment presents greater challenges for accurately estimating these measurement metrics compared to terrestrial settings [6, 7]. One common challenge is the noisy environment caused by high propagation loss. Another major challenge is the multipath effect, which causes signals to reach the receiving array through multiple paths, resulting in the signals from different paths becoming coherent.

Benefit from its distinguished robustness and low computational complexity, conventional beamforming (CBF) is widely adopted in underwater DOA estimation [8]. However, due to the Rayleigh constraints caused by the small array aperture, CBF results are often blurred with low spatial resolution [9]. Although the resolution can be improved by increasing the array aperture, it significantly increases deployment difficulty and compromises concealment in practical applications [10-12].

In recent years, deconvolution algorithms, originally developed for image restoration, have been applied to post-process CBF results to improve spatial resolution without expanding the array aperture [13-15]. Specifically, the CBF results with limited resolution are considered as a convolution of beam patterns and source intensity distributions with super resolution. Therefore, deconvolution algorithms attempt to recover the true source distributions from the CBF results to enhance resolution. Based on this idea, Yang successfully applied the Richardson-Lucy (R-L) deconvolution algorithm to CBF with a uniform line array (ULA) [16], and achieved narrower beamwidth and lower sidelobes level. Meanwhile, it retains the robustness of CBF under low signal-to-noise ratio (SNR) environment.

However, because of the nonlinear operation in constructing the spectrum convolution response, the above algorithms [13-16] can only handle scenarios where the received signals are incoherent. Their DOA estimations will be biased due to cross-term sidelobes when directly applied to actual underwater environments [17]. In addition, deconvolution beamforming can only utilize the statistical characteristics of the array receiving signals. In the application of integrated sonar and communication systems, or other collaborative systems that widely use wideband signals, the prior information of source signal waveform can be available. It has been demonstrated that the Cramer-Rao bound (CRB) for DOA estimation is significantly lower for signals with known waveforms compared to those without.

To address the DOA estimation problems for underwater wideband sources with known waveforms, a cross-correlation-based complex-valued sparse deconvolution beamforming (CC-SDB) is proposed in this paper. The main contributions of this paper are summarized as follows.

This work was supported by the Natural Science Foundation of China Grant No.52371352.

(1) Cross-correlation-based beamforming model for wideband signals is developed from the existing DOA estimation model. Due to the full utilization of prior waveform information, the new model maximizes the output SNR and enhances the robustness.

(2) Complex-valued sparse deconvolution beamforming is proposed to improve the estimation resolution of this model. The cross-term sidelobes caused by the non-linear operation in constructing the spectrum convolution response in the spatial domain are mitigated, so that the algorithm can handle coherent case.

Numerical simulations and underwater experiment were conducted to verify the effectiveness of CC-SDB. Its performance was evaluated against other conventional or deconvolution algorithms under various SNR and elements conditions, with the CRB introduced as a benchmark for comparison.

The rest of this paper is composed as follows. Section II describes the signal model in multipath environment. Section III describes deconvolution models in spatial domain and proposes CC-SDB. Sections IV and V show the performance of CC-SDB through numerical simulations and underwater experiments. Finally, Section VI concludes the paper and makes an expectation.

Notations: in subsequent chapters, vectors and matrices are denoted by lower-case and bold capital letters, respectively. $(\_)^T$, $(\_)^H$, $(\_)^*$ and $(\otimes)$ stand for transpose, conjugate transpose, complex conjugate and convolution, respectively.

II. Array Multipath Signal Model

We consider a ULA consisting of M isotropic hydrophones and use the first hydrophone as the reference array element. As shown in the left half of Fig.1, there are L propagation paths reaching the array, with DOA θ_l defined as the angle between the l-th $(l = 1,2,\cdots,L)$ path and the normal direction of the array, and with TOA t_l defined as the transmission time of the l-th path wave from the transmitter to the reference array element. As shown in the right half of Fig.1, the relative delay for the l-th path from the reference array element to the m-th$(m = 1,2,\cdots,M)$ array element is expressed as:

$$\tau_{m,l} = \frac{(m-1)d\sin\theta_l}{c} \tag{1}$$

where d is the distance between adjacent array elements, and c is the sound speed in water.

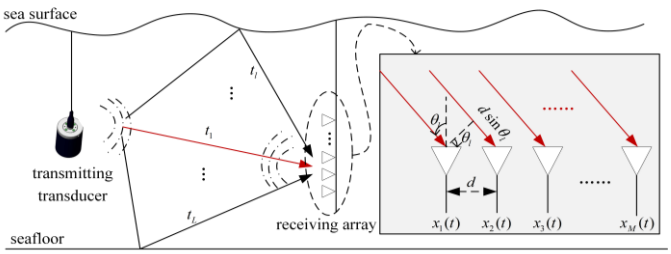

Fig. 1. Array signal model in a multipath environment.

The corresponding steering vector is

$$v_r = [v_{r1},\ldots,v_{rm},\ldots,v_{rM}]^T$$
$$v_{rm}(\theta,t) = e^{-j2\pi f(t)\tau_{m,l}(\theta)} \tag{2}$$

The hydroacoustic multipath channel impulse response model of the m-th array element can be expressed as:

$$h_m(t) = \sum_{l=1}^{L}\beta_l\delta(t-t_l-\tau_{m,l}) \tag{3}$$

where β_l is the attenuation of the l-th path.

The received signal of the m-th array element $x_m(t)$ is expressed as:

$$\begin{aligned} x_m(t) &= h_m(t)\otimes s_0(t) \\ &= \sum_{l=1}^{L}\beta_l s_0(t-t_l-\tau_{m,l}) + z_m(t) \\ &= \sum_{l=1}^{L}\beta_l s_{m,l}(t) + z_m(t) \end{aligned} \tag{4}$$

where $s_0(t)$ is the source signal, $s_{m,l}(t)$ denotes the l-th path signal received by m-th array element, $z_m(t)$ represents a white Gaussian noise vector and is not correlated with the source $s_0(t)$.

Hence, the array signal model in multipath environments can be represented in matrix form as follows:

$$\mathbf{X}(t) = \mathbf{H}(t)\otimes s_0(t) + \mathbf{Z}(t) \tag{5}$$

where $\mathbf{X}(t) = [x_1(t), x_2(t), \cdots, x_M(t)]^T$ represents the array receiving signal, $\mathbf{H}(t) = [h_1(t), h_2(t), \cdots, h_M(t)]^T$ represents the hydroacoustic multipath channel impulse response matrix, $\mathbf{Z}(t) = [z_1(t), z_2(t), \cdots, z_M(t)]^T$ represents a white Gaussian noise matrix.

III. The Proposed CC-SDB

A. Cross-Correlation-Based Beamforming Model

In the application of integrated sonar and communication system, the linear frequency modulation (LFM) source signal can be expressed as

$$s_0(t) = \sigma_s e^{j2\pi\alpha t + j\pi\beta t^2}, 0 \le t \le T \tag{6}$$

Where $\sigma_s$is the signal amplitude, α is the starting frequency, β is the chirp rate, and T is the signal time duration.

The steering vector of LFM signal is

$$v_r^1 = [v_{r1}^1,\ldots,v_{rm}^1,\ldots,v_{rM}^1]^T$$
$$v_{rm}^1(\theta,t) = e^{-j2\pi\tau_{m,l}(\theta)\left[f_0+\beta(t-t_l)-\frac{\beta}{2}\tau_{m,l}(\theta)\right]} \tag{7}$$

The steering vector v_r^1 depends not only on angle but also on the path transmission time t_l and the chirp parameters. The transmission time is hard to acquired and its estimation errors will affect the DOA estimation process.

To eliminate this impact, we develop the array signal model with a cross-correlation process, which can be expressed as:

$$\begin{aligned}\mathbf{R}_{xs}(t) &= \mathbf{X}(t) \otimes s_0(-t) \\ &= \mathbf{H}(t) \otimes s_0(t) \otimes s_0(-t) + \mathbf{Z}(t) \otimes s_0(-t) \\ &= \mathbf{H}(t) \otimes R_{ss}(t) + \mathbf{Z}(t) \otimes s_0(-t),\end{aligned} \tag{8}$$

where $\mathbf{R}_{xs}(t) = \left[R_{x_1 s}, \cdots, R_{x_m s}, \cdots, R_{x_M s}\right]^T$, $R_{x_m s}$ denotes the cross-correlation result of the m-th array element. If the noise term is ignored, it shows the cross-correlation matrix $\mathbf{R}_{xs}(t)$ can be expressed as the convolution of the source signal auto-correlation $R_{ss}(t)$ with the channel $\mathbf{H}(t)$.

Next, we demonstrate that the cross-correlation matrix $\mathbf{R}_{xs}(t)$ contains not only temporal information but also spatial information. The cross-correlation result $R_{x_m s}$can be expressed as

$$\begin{aligned}R_{x_m s} &= x_m(t) \otimes s_0(-t) \\ &= \sum_{l=1}^{L} \beta_l \delta(t - t_l - \tau_{m,l}) \otimes s_0(t) \otimes s_0(-t) + z_m(t) \otimes s_0(-t) \\ &= \sum_{l=1}^{L} \beta_l s(t - t_l - \tau_{m,l}) \otimes s_0(-t) + z_m(t) \otimes s_0(-t) \\ &= \sum_{l=1}^{L} \int_0^{f_s} \beta_l \left[S_l(f) e^{-j2\pi f(t_l + \tau_{m,l})} \right] \left[S_0^*(f) e^{j2\pi f t} \right] df + \eta_m(t) \\ &= \sum_{l=1}^{L} \int_0^{f_s} \beta_l \left[S_l(f) S_0^*(f) e^{-j2\pi f\left[t - (t_l + \tau_{m,l})\right]} \right] df + \eta_m(t) \\ &= \sum_{l=1}^{L} f_s |\sigma_l||\sigma_s| e^{-j2\pi f_c^l\left[t - (t_l + \tau_{m,l})\right]} \mathrm{sinc}\left\{ f_s \left[t - \left(t_l + \tau_{m,l} \right) \right] \right\} + \eta_m(t)\end{aligned} \tag{9}$$

where $\mathrm{sinc}(\cdot)$ is the sinc function; f_s is the sampling frequency; $s_0(t)$ is the normalized original wide-band chirp signal; and $S_l(f)e^{-j2\pi f(t_l+\tau_{m,l})}$ and $S_0^*(f)$ are the FT of $s\left(t - t_l - \tau_{m,l}\right)$ and $s_0(t)$, respectively. The center frequency of the l-th path signal f_c^l can be accurately estimated by calculating the spectral centroid of $R_{x_m s}$.

$$\hat{f}_c^l = \frac{\int_0^{f_s} f \cdot \left| X_m(f) S_l^*(f) \right| df}{\int_0^{f_s} \left| X_m(f) S_l^*(f) \right| df} \tag{10}$$

where the spectral centroid is the center of gravity of the spectrum.

Cross-correlation process compresses the signal, yields significant peaks, and maximizes output SNR, resulting in robust performance of the proposed scheme.

In (9), the energy of $R_{x_m s}$ is concentrated at $t_l + \tau_{ml}$ in the time domain. The maximum value of $R_{x_m s}$ is found at time index $\hat{t}_l$ as follows:

$$\hat{t}_l = \frac{1}{M} \sum_{M=1}^{M} \underset{t}{argmax}\left\{ \left| R_{x_m s} \right| \right\} \tag{11}$$

The value of $R_{x_m s}$ at $\hat{t}_l$ can then be expressed as

$$\begin{aligned}R_{x_m s}\left(\hat{t}_l\right) &= \sum_{l=1}^{L} f_s |\sigma_l||\sigma_s| e^{j2\pi f_c^l\left[\left(\hat{t}_l - t_l\right) + \tau_{m,l}\right]} \\ &\quad \times \mathrm{sinc}\left\{ f_s \left[\left(\hat{t}_l - t_l \right) + \tau_{m,l} \right] \right\} + \eta_m(t) \\ &\approx \sum_{l=1}^{L} f_s |\sigma_l||\sigma_s| e^{j2\pi f_c^l\left(\tau_{m,l}\right)} + \eta_m(t)\end{aligned} \tag{12}$$

where $\mathrm{sinc}\left\{ f_s\left[\left(\hat{t}_l - t_l \right) + \tau_{m,l} \right] \right\} \approx 1$.

Based on formula (9)(12), it has

$$R_{x_m s} = R_{x_1 s} \cdot v_{rm}^0(\theta) = R_{x_1 s} e^{-j2\pi f_c^l \tau_{m,l}} \tag{13}$$

Different from the time-varying steering vector v_r^1, the cross-correlation-based steering vector $v_r^0 = [v_{r1}^0, \ldots, v_{rm}^0, \ldots, v_{rM}^0]^T$ depends only on the unknown multipath DOA. Thus, the DOA estimation can be carried out without estimating TOA. This means that temporal and spatial information have been decoupled, and their errors will not be transmitted to each other.

The cross-correlation-based CBF (Cc-CBF) is performed with temporal peaks data is expressed as:

$$\begin{aligned}P_{\theta-\tau} &= \left| \left(v_r^0 \right)^H \mathbf{X} \otimes s_0 \right|^2 \\ &= \left[\left(v_r^0 \right)^H \mathbf{X} \otimes s_0 \right] \left[(\mathbf{X} \otimes s_0)^H v_r^0 \right] \\ &= \left(v_r^0 \right)^H \mathbf{R}_{xs} \left(\mathbf{R}_{xs} \right)^H v_r^0\end{aligned} \tag{14}$$

The cross-correlation-covariance matrix $\mathbf{R} = \mathbf{R}_{xs}(\mathbf{R}_{xs})^H$ contains the temporal information of signals, and the steering vector v_r^0 contains spatial information. Therefore, joint TOA-DOA estimation can be obtained from $P_{\theta-\tau}$.

However, the resolution of obtained raw spectrum is limited by signal bandwidth and Rayleigh constraints. In the next part, a post-processing method based on deconvolution algorithm with sparseness and continuity constraints will be introduced to improve the resolution.

B. Complex-valued Sparse Deconvolution Algorithm

In the spatial domain, the cross-correlation-based beamforming intensity in the desired direction $\theta_r \in (-\pi/2, \pi/2)$ can be expressed as follows:

$$\begin{aligned}B(\sin\theta_r) &= (v_r^0)^H \mathbf{R}_{xs} \\ &= \sum_{l=1}^{L} \frac{f_s |\sigma_l||\sigma_s|}{M} \sum_{m=1}^{M} e^{\frac{j2\pi(m-1)d(\sin\theta_r - \sin\theta_l)}{\lambda_0}} \mathrm{sinc}\left\{ f_s \left[t - \left(t_l + \tau_{m,l} \right) \right] \right\} \\ &= \sum_{l=1}^{L} \frac{f_s |\sigma_l||\sigma_s|}{M} e^{\frac{j\pi(m-1)du_{rl}}{\lambda_0}} \frac{\sin c(M\pi d u_{rl}/\lambda_0)}{\sin c(\pi d u_{rl}/\lambda_0)}\end{aligned} \tag{15}$$

where $u_{rl} = \sin\theta_r - \sin\theta_l$,$\lambda_0$ is reference wavelength. It has been also observed that there is no grating lobe when $d = \frac{\lambda_0}{2}$, which we have considered as the optimal design spacing for the array antenna elements in the smart antenna [18].

Clearly, $B(\sin\theta_r)$ can be regarded as the superposition of L propagation paths in the direction θ_r through the beam pattern in the complex-value domain.

The spectrum of Cc-CBF can be expressed as follows:

$$B_p(\sin\theta_r) = |B(\sin\theta_r)|^2$$
$$= \sum_{l=1}^{L}|s|^2\left|\frac{\sin c\,(M\pi du_{rl}/\lambda_0)}{\sin c\,(\pi du_{rl}/\lambda_0)}\right|^2 + \sum_{l=1}^{L}\sum_{\substack{i=1\\ i\neq l}}^{L} CS_{rli}\,,$$
$$\approx \sum_{l=1}^{L}|s|^2\left|\frac{\sin c(M\pi du_{rl}/\lambda_0)}{\sin c(\pi du_{rl}/\lambda_0)}\right|^2 \quad (16)$$

It is worth noting that only when the signal incident is incoherent ($s_l s_i^{\,*} = 0$) can the sum of the cross-terms CS_{rli} be neglected. And this is the nonlinear operation in the construction of spectral convolution response.

$$CS_{rli} = s_l {s_i}^{*} e^{\frac{j\pi(m-1)du_{rl}}{\lambda}} \frac{\sin c(M\pi du_{rl}/\lambda_0)}{\sin c(\pi du_{rl}/\lambda_0)} \cdot \frac{\sin c(M\pi du_{ri}/\lambda_0)}{\sin c(\pi du_{ri}/\lambda_0)}. \quad (17)$$

In the complex-value domain, the beamforming spectrum in (15) can be written as the convolution between the beam pattern $B_{psf}(\sin\theta_r - \sin\vartheta)$ and the source intensity distribution $S_p(\sin\vartheta)\vartheta = [\vartheta_1, \vartheta_1, \cdots, \vartheta_N] \in (-\pi/2, \pi/2)$ is the traversal of the possible DOA, N is the beam number.

The cross-correlation-based beamforming intensity of the desired direction θ_r is:

$$\begin{aligned} B(\sin\theta_r) &= \int_{-1}^{1} B_{psf}(\sin\theta_r - \sin\vartheta) S_p(\sin\vartheta) d\sin\vartheta \\ &= B_{psf}(\sin\theta_r) \otimes S_p(\sin\theta_r) \end{aligned} \quad (18)$$

The expression of the beam pattern is:

$$B_{psf}(\theta_r) = \frac{\sin c(M\pi d\theta_r/\lambda)}{\sin c(\pi d\theta_r/\lambda)} \quad (19)$$

and the source intensity distribution is given by the $S_p(\sin\theta_r) = \sum_{l=1}^{L}|s|^2\delta(\sin\theta_r - \sin\theta_l)$.

Generally, it is also possible to express the process in (18) through the matrix multiplication in (20).

$$\mathbf{w}_{spa} q_{spa} = b_{spa} \quad (20)$$

where $B_p(\sin\theta_r)$ and $S_p(\sin\theta_r)$ can be regarded as the elements in b_{spa} and q_{spa} respectively. And $\mathbf{w}_{spa}$ is a square matrix, with each column corresponding to a beam pattern in a certain direction ϑ:

$$\mathbf{w}_{spa} = \begin{bmatrix} B_{psf}(\sin\theta_{r1} - \sin\vartheta_1) & B_{psf}(\sin\theta_{r1} - \sin\vartheta_2) & \cdots & B_{psf}(\sin\theta_{r1} - \sin\vartheta_N) \\ B_{psf}(\sin\theta_{r2} - \sin\vartheta_1) & B_{psf}(\sin\theta_{r2} - \sin\vartheta_2) & \ddots & B_{psf}(\sin\theta_{r2} - \sin\vartheta_N) \\ \vdots & \vdots & \ddots & \vdots \\ B_{psf}(\sin\theta_{rN} - \sin\vartheta_1) & B_{psf}(\sin\theta_{rN} - \sin\vartheta_2) & \cdots & B_{psf}(\sin\theta_{rN} - \sin\vartheta_N) \end{bmatrix} \quad (21)$$

From the above derivation, the cross-correlation-based deconvolution models for DOA estimation is $\mathbf{w}_{spa} q_{spa} = b_{spa}$. Only a limited number of multipaths can reach the array, therefore, the number of multipath is much less than the beam number N and the potential time delays number Q, so q_{spa} is sparse.

The deconvolution algorithm with the ℓ_1-norm sparse constraints to post-process the raw map is expressed as:

$$\text{minimize } \|q_{spa}\|_1 \text{ subject to } b_{spa} = \mathbf{W}_{spa} q_{spa}. \quad (22)$$

Normally, the target function (22) is equivalent to the following expression:

$$f(x) = \frac{1}{2}\|\mathbf{W}q_{spa} - b_{spa}\|_F^2 + \eta\|\mathbf{D}q_{spq}\|_1, \quad (23)$$

where $\|\bullet\|_F$ denotes the Frobenius norm. η denotes the regularization coefficient. The value of η is not sensitive to the true source distribution and is generally considered as the mean signal power [19]. Because the beamforming power between adjacent grids should be similar, the difference matrix **D** is used to retain this continuity [20]. **D** is generally expressed as a first-order difference matrix:

$$\mathbf{D} = \begin{bmatrix} 1 & -1 & 0 & \cdots & 0 \\ 0 & 1 & -1 & \ddots & \vdots \\ 0 & \ddots & \ddots & \ddots & 0 \\ \vdots & \ddots & \ddots & 1 & -1 \\ 0 & \cdots & \cdots & 0 & 1 \end{bmatrix}. \quad (24)$$

As for the non-negative convex optimization problem (23), it can be solved by using FISTA[21]. Fig.2 shows the flow chart of proposed CC-SDB.

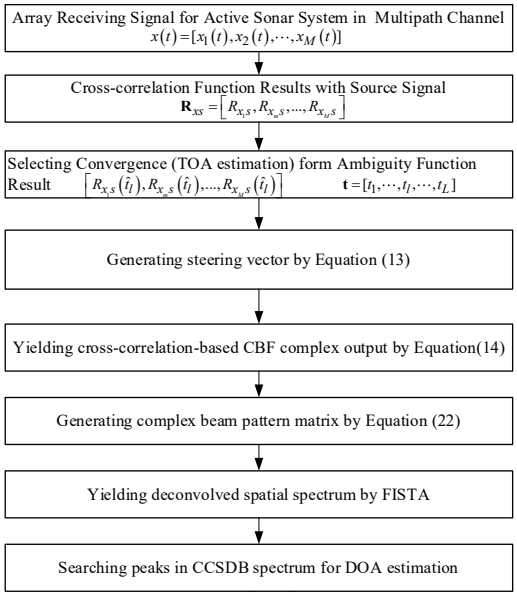

Fig. 2. Sparse deconvolution post-processing flow chart.

IV. Simulation Results

In this section, the performance of CC-SSB is verified. Unless otherwise specified, the array comprises eight omnidirectional hydrophones at half-wavelength intervals. The beam pattern in the spatial domain satisfies the shift-invariant property when it is a sine function of the DOA, so the beam

sweep range is from -1 to 1 with an increment of 0.001. The source signal is an LFM signal with a frequency range of 6-9 kHz, a signal length of 50 ms, and a sampling rate of 96 kHz.

A. Performance versus SNR in the Case of High-correlation DOA

In the first simulation, we consider the LFM source reaching the array along two paths. The line-of-sight (LOS) path is from DOA of -3° and TOA of 9ms, while another non-line-of-sight (NLOS) path is from DOA of 3° and TOA of 11ms. The correlation between these two paths is 0.95, and SNR is varying from -20dB to 20dB in 5dB increments. As shown in Fig.3(a), because of path combinations in a two-way channel, the receiving signals converge into only three peaks on the ambiguity-function map. Fig.3(b) is an enlarged display version near these peaks which represent path combinations of LOS-LOS, LOS-NLOS (completely overlapping with NLOS-LOS), and NLOS-NLOS, respectively. To demonstrate the effectiveness of the proposed algorithm, we compared its performance with Cc-CBF, RL based on incoherent model(16), DAMAS based on coherent model(15), and frequency invariant beamforming (FIB) in the aspect of main-lobe width (MW), side-lobe level (SL), resolution probability (RP), root-mean-square-error (RMSE).

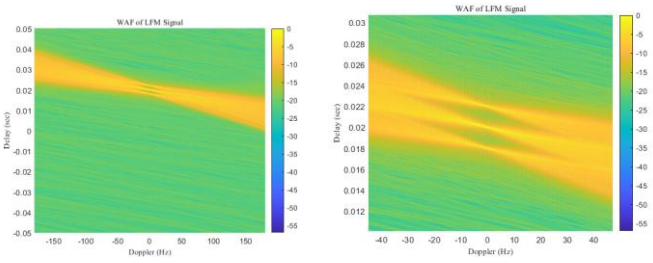

(a) Path combination (b) Zoom-in version

Fig. 3. Wideband ambiguity function of receiving signal.

Fig.4(a) shows the spectrum results of a Monte Carlo simulation at 0dB. Due to the angle interval being set to be smaller than the main-lobe width of Cc-CBF and FIB, they fail to distinguish the two paths at all SNRs. Fig.4(b) provides an enlarged view near these spectrum peaks. The order of peak offset from largest to smallest is FIB≈Cc-CBF>>DAMAS>RL>CC-SDB. The order of side-lobe level from highest to lowest is : FIB≈Cc-CBF>>RL>DAMAS>CC-SDB.

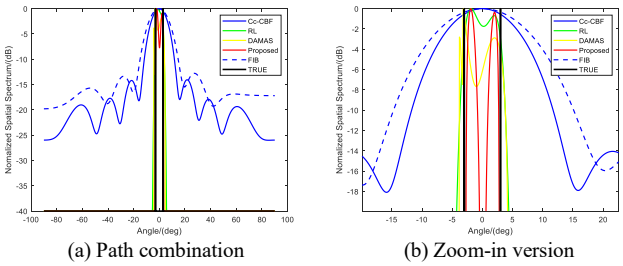

(a) Path combination (b) Zoom-in version

Fig. 4. Spatial spectrum of different algorithm.

The performance versus SNR in terms of RMSE, RP, SL, MW is illustrated in Fig.5, and the CRB provides an algorithm-independent benchmark for comparison reference. Fig.5(a) shows that the RMSE of each algorithm decreases as the SNR increases. The DOA estimation performance of CC-SDB remains within 1° at different SNR, which is closest to CRB. The performance of Cc-CBF is not given due to the inability to distinguish the two paths shown in Fig.5(b). CC-SDB can achieve a resolution probability of 100% with only 7 elements at high-correlation case and 3 elements at -15dB, while RL, and DAMAS require higher SNR to achieve the same resolution probability. Fig.5(c)(d) shows the variation of side-lobe level and main-lobe width of each algorithm within the simulated SNR range. Overall, the performance of CC-SDB based on coherent model in various aspects are competent at this high-correlation case, demonstrating extremely effectiveness and robustness from cross-correlation.

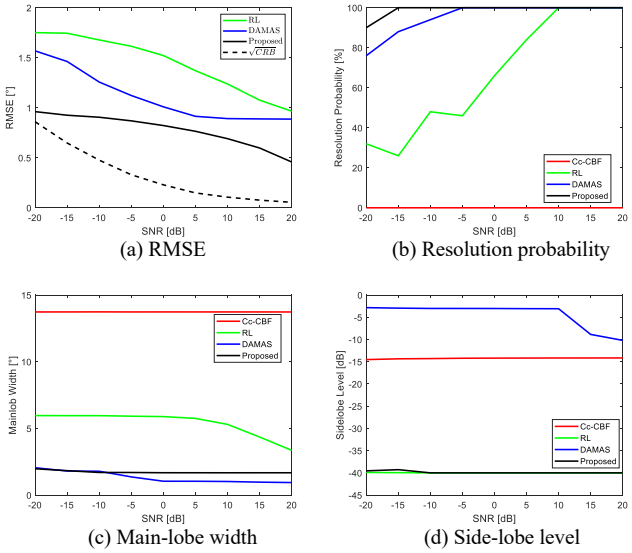

(a) RMSE (b) Resolution probability

(c) Main-lobe width (d) Side-lobe level

Fig. 5. Performance of different algorithms versus SNR.

B. Performance Versus Sensor Number

The second simulation discusses performance versus different sensor numbers at 0 dB in the high-correlation case. Based on Fig.6(b), CC-SDB and DAMAS can achieve a resolution probability of 100% with only 7 elements at high-correlation case, while RL requires more elements to achieve the same resolution probability. On the premise of successfully distinguishing between two paths, as shown in Fig.6(a), CC-SDB has the most accurate DOA estimation performance, RL and DAMAS come second similarly. This indicates that Cc-SDB can achieve successful resolution of adjacent paths with fewer array elements under low SNR conditions, and can better adapt to marine environments with limited array elements and strong noise.

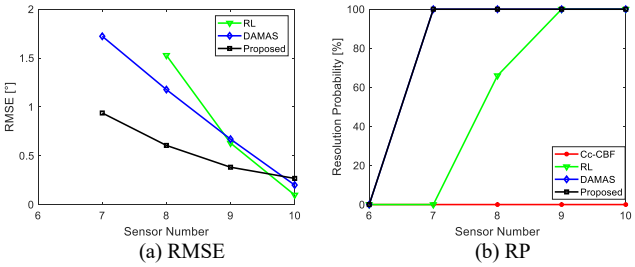

(a) RMSE (b) RP

Fig. 6. Performance of different algorithms versus sensor number.

V. Experimental Verification

To validate the performance of T-SSD, experiments were conducted at Jingye Lake in Tianjin, China. After the hydrologic exploration using the Valeport miniSVP, the average depth of the lake was determined to be approximately 5 meters, and the speed of sound was 1476 m/s. The experimental scene is depicted in Fig. 7. To ensure the received signals are coherent, two identical transducers with type of 715-CT-22 send the same source signal. The hydrophone array consists of seven Brüel & Kjær 8104 hydrophones with an array spacing of 0.05 m.

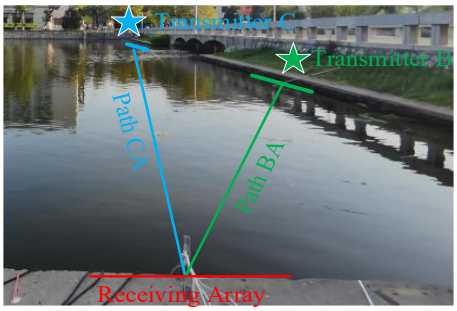

Fig. 7. Experimental scene.

Both the array and the transducers are placed at 1.5 m depth, and the hydrophone array is placed horizontally to avoid receiving unknown multipath signals form seafloor and surface as much as possible. Measured by the NTS-382R6 total station, one transducer labelled as Target B is placed at 21.31° and 64.95 meters from the array, and the other labelled as Target 2 is placed at 1.83° and 10.37 meters from the array, so that the far-field conditions are satisfied [22]. The source signal is 13-17 kHz LFM with a duration of 50ms. At the receiving array, the sampling rate is 200 kHz, and the received signal is processed by a filter with a passband of 10-20 kHz, and a gain of 6.7dB. The detailed diagram of the experimental instruments is shown in Fig. 8.

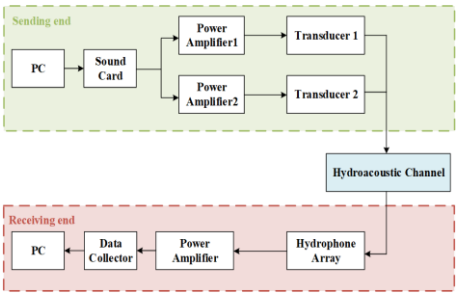

Fig. 8. Diagram of the experiment instruments.

Fig. 9 illustrates the estimation results of these two target by using each algorithm. As can be seen, since the RL algorithm is based on incoherent models, sidelobes occur because of the interference from cross-terms. While CC-SDB can better compress the main-lobe width and reduce the side-lobe level, making it easier to extract the direct paths of various sources in the horizontal plane. This indicates the effectiveness of the algorithm proposed in this paper in estimating the DOA of coherent sources in cooperative detection scenarios.

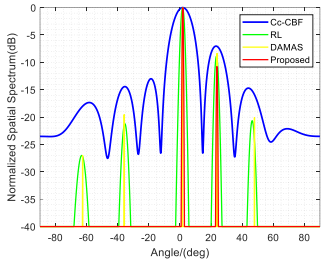

Fig. 9. Estimation results of the coherent signal by different methods.

VI. Conclusion

This paper proposes a cross-correlation-based complex-valued sparse deconvolution beamforming (CC-SDB) for wideband source used in active sonar system in multipath-rich environment. to realize accurate and robust DOA estimation. The first contribution is to apply cross-correlation function in the development of conventional DOA estimation model, which maximizes the output SNR and enhances the robustness of the algorithm. The second contribution is to post-process this model by using the characteristic of sparse convolution to suppress the main-lobe width and the sidelobes levels to obtain high-resolution estimation results. The numerical simulations and underwater experiments show that CC-SDB can get the most stable and satisfying estimation performance at low SNR and small array aperture.

CC-SDB can be applied to various applications such as sound source localization, multipath signal recognition, and target detection. In the future, we plan to introduce additional norm constraints in CC-SDB to achieve higher accuracy in DOA estimation. Furthermore, we aim to combine these constraints with fast algorithms to reduce computational complexity, making the approach suitable for navigation fields with higher real-time requirements. Leveraging machine learning and artificial intelligence to enhance CC-SDB is a significant trend, as these technologies can effectively handle complex scenarios involving impulsive noise and nonlinearities. This approach holds great potential for applications on the Internet of Things (IoT), autonomous vehicles, smart cities, and medical fields.

References

[1] M. Alibakhshikenari *et al.*, "Study on on-Chip Antenna Design Based on Metamaterial-Inspired and Substrate-Integrated Waveguide Properties for Millimetre-Wave and THz Integrated-Circuit Applications," *Journal of Infrared, Millimeter, and Terahertz Waves,* vol. 42, no. 1, pp. 17-28, 2021/01/01 2021, doi: 10.1007/s10762-020-00753-8.

[2] M. Alibakhshikenari *et al.*, "Bandwidth and gain enhancement of composite right left handed metamaterial transmission line planar antenna employing a non foster impedance matching circuit board," *Scientific Reports,* vol. 11, no. 1, p. 7472, 2021/04/02 2021, doi: 10.1038/s41598-021-86973-x.

[3] E. L. Chuma, L. L. B. Roger, G. G. de Oliveira, Y. Iano, and D. Pajuelo, "Internet of Things (IoT) Privacy–Protected, Fall-Detection System for the Elderly Using the Radar Sensors and Deep Learning," 2020.

[4] B. Zhang, X. Hou, Y. Yang, L. Yang, and Y. Wang, "A Fast Variational Bayesian Adaptive Extended Kalman Filter for Robust Underwater Direction-of-Arrival Tracking," *IEEE Sensors Journal,* vol. 23, no. 13, pp. 14709-14720, 2023, doi: 10.1109/JSEN.2023.3275318.

[5] H. Chen, J. Zhang, B. Jiang, X. Cui, R. Zhou, and Y. Zhang, "Multi-source underwater DOA estimation using PSO-BP neural network

based on high-order cumulant optimization," *China Communications,* vol. 20, no. 12, pp. 212-229, 2023, doi: 10.23919/JCC.ea.2021-0031.202302.

[6] Q. I. Bingbing, "DOA estimation of the coherent signals using beamspace matrix reconstruction," *Signal Processing,* vol. 191, p. 108349, 2022, doi: https://doi.org/10.1016/j.sigpro.2021.108349.

[7] L. Cheng, Y. Li, L. Zou, and Y. Qin, "DOA Estimation for Highly Correlated and Coherent Multipath Signals with Ultralow SNRs," *International Journal of Antennas and Propagation,* vol. 2019, no. 1, p. 2837315, 2019, doi: https://doi.org/10.1155/2019/2837315.

[8] Z. Xu, H. Li, and K. Yang, "A Modified Differential Beamforming and Its Application for DOA Estimation of Low Frequency Underwater Signal," *IEEE Sensors Journal,* vol. 20, no. 16, pp. 8890-8902, 2020, doi: 10.1109/JSEN.2020.2988025.

[9] C. Yang, Y. Wang, Y. Wang, D. Y. Hu, and H. Guo, "An improved functional beamforming algorithm for far-field multi-sound source localization based on Hilbert curve," (in English), *APPLIED ACOUSTICS,* vol. 192, APR 2022, Art no. 108729, doi: 10.1016/j.apacoust.2022.108729.

[10] M. M. Fakharian, M. Alibakhshikenari, C. H. See, and R. Abd-Alhameed, "A high gain multiband offset MIMO antenna based on a planar log-periodic array for Ku/K-band applications," *Scientific Reports,* vol. 12, no. 1, p. 4044, 2022/03/08 2022, doi: 10.1038/s41598-022-07866-1.

[11] M. Alibakhshikenari *et al.*, "Singular Integral Formulations for Electrodynamic Analysis of Metamaterial-Inspired Antenna Array," *IEEE Antennas and Wireless Propagation Letters,* vol. 20, no. 2, pp. 179-183, 2021, doi: 10.1109/LAWP.2020.3043380.

[12] M. Alibakhshikenari *et al.*, "Novel Concentric Hexagonal-Shaped RFID Tag Antenna With T-Shaped Stub Matching," *IEEE Journal of Radio Frequency Identification,* vol. 6, pp. 112-120, 2022, doi: 10.1109/JRFID.2021.3124966.

[13] D. Robert, *Extensions of DAMAS and Benefits and Limitations of Deconvolution in Beamforming*.

[14] O. Lylloff, E. Fernández-Grande, F. Agerkvist, J. Hald, E. Tiana Roig, and M. S. Andersen, "Improving the efficiency of deconvolution algorithms for sound source localization," *The journal of the acoustical society of America,* vol. 138, no. 1, pp. 172-180, 2015.

[15] L. Shen, Z. Chu, L. Tan, D. Chen, and F. Ye, "Improving the Sound Source Identification Performance of Sparsity Constrained Deconvolution Beamforming Utilizing SFISTA," *Shock and Vibration,* vol. 2020, no. 1, p. 1482812, 2020, doi: https://doi.org/10.1155/2020/1482812.

[16] T. Yang, "Deconvolved conventional beamforming for a horizontal line array," *IEEE Journal of Oceanic Engineering,* vol. 43, no. 1, pp. 160-172, 2017.

[17] Z. Chu and Y. Yang, "Comparison of deconvolution methods for the visualization of acoustic sources based on cross-spectral imaging function beamforming," *Mechanical Systems and Signal Processing,* vol. 48, no. 1, pp. 404-422, 2014/10/03/ 2014, doi: https://doi.org/10.1016/j.ymssp.2014.03.012.

[18] A. S. Oluwole and V. M. Srivastava, "Analysis and Synthetic Model of Adaptive Beamforming for Smart Antenna Systems in Wireless Communication," *J. Commun.,* vol. 13, no. 8, pp. 436-442, 2018.

[19] M. Wu and C. Hao, "Super-Resolution TOA and AOA Estimation for OFDM Radar Systems Based on Compressed Sensing," *IEEE Transactions on Aerospace and Electronic Systems,* vol. 58, no. 6, pp. 5730-5740, 2022, doi: 10.1109/TAES.2022.3178393.

[20] M. Donatelli and L. Reichel, "Square smoothing regularization matrices with accurate boundary conditions," (in English), *JOURNAL OF COMPUTATIONAL AND APPLIED MATHEMATICS,* vol. 272, pp. 334-349, DEC 15 2014, doi: 10.1016/j.cam.2013.08.015.

[21] A. Beck and M. Teboulle, "A fast Iterative Shrinkage-Thresholding Algorithm with application to wavelet-based image deblurring," in *2009 IEEE International Conference on Acoustics, Speech and Signal Processing*, 19-24 April 2009 2009, pp. 693-696, doi: 10.1109/ICASSP.2009.4959678.

[22] J. J. Handfield, R. M. Rao, and S. A. Dianat, "Near-field MVDR source localization," presented at the WIRELESS SENSING AND PROCESSING III, 2008.